Free-vibration analysis of space vehicle structures made by composite materials

Free-Vibration Analysis of Space Vehicle Structures made by Composite materials.

T. Cavallo[a]*, E. Zappino[a]†, E. Carrera[a]‡,
[a] MUL^2 Group, Department of Mechanical and Aerospace Engineering, Politecnico di Torino, Corso Duca degli Abruzzi 24, 10129 Torino, Italy.

September 8, 2017

Submitted to: Composite Structures - Prof. Narita Special Issue

Author for correspondence:
E. Zappino, PhD, Research assistant,
Department of Mechanical and Aerospace Engineering,
Politecnico di Torino,
Corso Duca degli Abruzzi 24,
10129 Torino, Italy,
tel: +39 011 090 6887,
fax: +39 011 090 6899,
e-mail: enrico.zappino@polito.it

*PhD student, e-mail: tommaso.cavallo@polito.it
†Research assistant, e-mail: enrico.zappino@polito.it
‡Professor of Aerospace Structures and Aeroelasticity, e-mail: erasmo.carrera@polito.it

Abstract

This work investigates the effects of composite materials and non-structural masses on the dynamic behavior of space structure components and whole space vehicle. A refined one-dimensional model has been used in the analyses, and the effects of composite materials and of the fuel mass introduced as non-structural masses have been considered. The adopted refined one-dimensional Finite Element Model has been developed using the Carrera Unified Formulation. This numerical tool allows to develop a variable kinematic displacement field over the beam cross-section, that is, a set of Lagrange (LE) expansions polynomials was adopted for the cross-sectional displacement field approximation. The use of such one-dimensional models leads to the so-called component-wise (CW) approach in which stiffeners and plate are modeled using the same one-dimensional kinematic. Static and free vibration analysis of space structural components and complete space structures have been performed. Both compact and thin-walled structural configurations have been considered. The results have been assessed using analytical solutions or refined three-dimensional Finite Element Models. Composite materials and non-structural masses, e.g. the fuel mass or payload, have been included in the analysis. The results show the capability of the present model to provide a quasi three-dimensional solution with a low computational cost. The refined kinematic allows composite materials to be investigated accurately.

1 Introduction

Reinforced structures are thin-walled structures reinforced using longitudinal stringers and transversal ribs joined using different technologies. In some aeronautical structures, such as fuselage components, stringers are joined to skins using riveting techniques. In this case, stringers and skins are joined only in the area where there the rivet is applied and there is not structural continuity between the stringer and the panel. In other applications, components are welded using an additional material characterized by defined chemical and mechanical properties. The welding technique ensures the structural continuity in a limited area but also may include structural defects and thermal deformations. In the recent years, the milling techniques and the use of composite materials allow reinforced structures to be obtained as a unique body, without the need to include additional components. The use of these techniques improves the mechanical performances of the structures and may reduce their weight but, in contrast, they are much more expensive than riveting and welding.

In the last century, different approaches have been introduced to study reinforced structures with the purpose of investing the static and dynamic behavior. The complex shape of a generic reinforced structure requires the introduction of geometrical and kinematic approximation to be studied with classical numerical models. The simplified model proposed by Timoshenko [1] deals with the analysis of complex structures. An equivalent orthotropic homogeneous panel with constant thickness is obtained by smearing-out the stiffness properties of the ribs over the plate considering the ribs closely and evenly spaced. The use of this method requires the contribution of each component to be evaluated locally and then it must be superimposed to the global properties of the panel. This approach provides accurate results for closely and equally spaced reinforcements while it is not able to describe the local effects due to evenly spaced stringers. When the number of ribs used to reinforce the structure decreases, the plate and rib components should be considered separately, and the congruence between them should be imposed. Many works, see [2, 3, 4, 5], shown that in this case the solutions for the plate and stringers could be evaluated separately, considering the external forces as well as the interface forces, due to the coupling between the components. Leissa [6, 7] presented the first work on stiffened plates and stiffened cylindrical shells. Junger and Feit [8] proposed an improved smearing technique considering the reaction forces on a plate due to both the translational and rotary inertia of regularly spaced stiffeners.

The introduction of the Finite Element Method (FEM) [9] was a great step foreword in the analysis of complex structures. Although different FEM approaches exist, they all share the common idea of discretizing the physical domain of the whole structure into a set of discrete sub-domains, which are usually called elements. An early FEM solution was presented by Hrennikoff [10] in 1941. Two years later the solution of a simple square structure was published by Courant [11]. In 1973 an important contribution for the FEM was towards by Strang and Fix [12]. One of the classical problem in the FEM is the need for a large storage capacity and high computational power when large structures are considered. In particular, the solid elements, or three-dimensional elements, are very accurate because their kinematics is not afflicted by any fundamental assumptions but, unfortunately, they require a large number of unknowns (degrees of freedoms, DOFs), and this leads to high computational costs. The use simplified structural models, such as beam (one-dimensional) and plate (two-dimensional) models may reduce the computational costs but, in contrast, the results are accurate only when the fundamental assumptions are fulfilled. In 1976 the vibration response of the Space

Shuttle solid boosters has been used to investigate using a 1/8 scaled model. The experimental results have been successfully compared whit those obtained using two reduced FE models built using only plate or beam elements. In 2000, the FEM has been used for the validation of an aircraft fuselage structures [13]. In 2011 two FE reduced models have been used to characterize the dynamic behavior of the boosters for the launcher Arian V [14]. The first FE model has been built using only beam elements, while the second FE model includes shell and beam elements for the structure and solid elements for the fuel. One year later [15], both shell and solid elements have been used to investigate the dynamic response of the solid propellant of the Arian V including a linear viscoelastic material with frequency dependent mechanical properties.

In this research area, the Carrera Unified Formulation (CUF) has contributed to analysing complex structures using refined structural theories able to provide accurate solutions with low computational costs.

The CUF is a mathematical tool able to derive high-order models in a compact form. The theoretical formulation and some applications can be found in the different works [16, 17, 18, 19, 20, 21].

The use of the component-wise (CW) approach [22], makes it possible to study very complex structures using a unique one-dimensional formulation. The effectiveness of the CW approach was showed for both static [22] and dynamic [23] analyses of simple structures.

In 2013, the CUF permitted to perform the free vibration analysis of composite simple beam models using refined theory [24].

Recently, the analysis of the problems due to the modelling of the area between skin and stringer are carried out highlighting the limit of the reduced $1D/2D$ FE models [25].

A significant breakthrough has meant that complex reinforced structures to be analysed, isotropic curved panels and reinforced cylinder, in static [26] and dynamic [27] analyses.

This approach has been used to study a luncher made in isotropic material [28] with a central body and two lateral boosters. The effect of the solid fuel consumption on the dynamic behaviour of the proposed isotropic launcher has been also considered [29].

The present work has the purpose to extend the use of refined one-dimensional models to the analysis of complex composite reinforced structures. The first part of this paper introduces the one-dimensional structural model based on the use of Lagrange expansion (LE) to approximate the cross-section. The second part has the purpose of investigating the effect of the coupling of composite materials and non-structural masses on the dynamic behaviour of complex reinforced structures. Different FE models from the commercial $Nastran$ code have been used to compare the results with those from the $1D - CUF$ models.

2 Refined one-dimensional models

The structural models used in the present work are derived using the Carrera Unified Formulation. Details about 1D formulation derived using the CUF can be found in [30].

2.1 Adopted LE displacement fields

Fig.1 shows the adopted coordinate frame, where along the beam axis, the $y - axis$, the beam length is L. The displacement vector can be written as:

$$\boldsymbol{u}(x, y, z) = \left\{ \begin{array}{ccc} u_x & u_y & u_z \end{array} \right\}^T \tag{1}$$

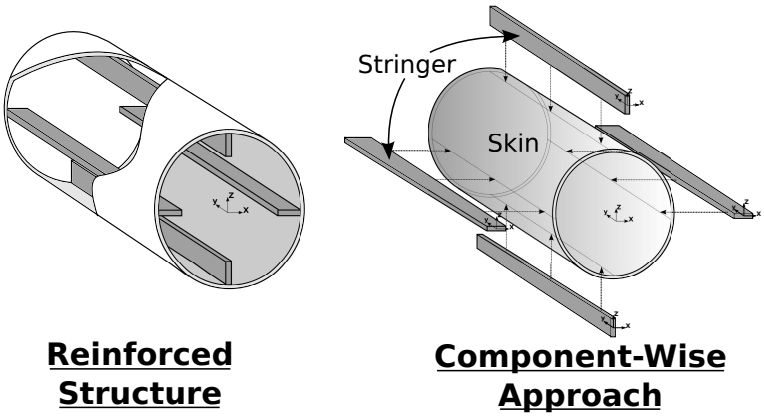

Figure 1: Component-Wise approach for reinforced structures.

The superscript T denotes transposition. Likewise for stress, σ, and strain, ϵ, components can be introduced as follows:

$$\boldsymbol{\sigma} = \left\{ \begin{array}{cccccc} \sigma_{xx} & \sigma_{yy} & \sigma_{zz} & \sigma_{xy} & \sigma_{xz} & \sigma_{yz} \end{array} \right\}^T \tag{2}$$

$$\boldsymbol{\epsilon} = \left\{ \begin{array}{cccccc} \epsilon_{xx} & \epsilon_{yy} & \epsilon_{zz} & \epsilon_{xy} & \epsilon_{xz} & \epsilon_{yz} \end{array} \right\}^T \tag{3}$$

Linear strain-displacement relations are used,

$$\boldsymbol{\epsilon} = \mathbf{D}\boldsymbol{u} = \left([\mathbf{D}_y] + [\mathbf{D}_\Omega] \right) \boldsymbol{u} \tag{4}$$

$\mathbf{D}$ is a differential operator and its explicit form can be found in [30]. $\mathbf{D}_y$ and $\mathbf{D}_\Omega$ represent the differential operator on beam axis y and on the beam cross-section, respectively. The material is isotropic, the Hooke's law can be written as:

$$\boldsymbol{\sigma} = \mathbf{C}\boldsymbol{\epsilon} \tag{5}$$

In the framework of the CUF [20], [30], for a 1D problem, the displacement field $\mathbf{u}$ is written as the product of two functions, a cross-sectional expanding function F_τ and the generalized displacement vector unknown $\mathbf{u}_\tau$ on the y-axis:

$$\boldsymbol{u}(x, y, z) = F_\tau(x, z)\mathbf{u}_\tau(y) \tag{6}$$

where index τ ranges from 1 to the number of terms of the expansion of order N.

2.1.1 Lagrange expansion polynomials (LE)

When Lagrange models are used to realize the cross-section of the 1D refined models, different types of Lagrange elements can be used, four-points LE-4, nine-points LE-9, sixteen-points LE-16 Lagrange Elements. The nine-point LE 9 cross-section polynomial set are adopted in this paper, due to their accuracy with respect to the LE-4 and LE-16. Some details related to the convergence analysis can be found in [25]. The isoparametric formulation is exploited to deal with arbitrary cross-section shaped geometries. For instance, LE-9 interpolation functions are:

$$\begin{gathered} F_\tau = \tfrac{1}{4}(r^2 + r\, r_\tau)(s^2 + s\, s_\tau) \qquad \tau = 1, 3, 5, 7 \\ F_\tau = \tfrac{1}{2}s_\tau^2(s^2 - s\, s_\tau)(1 - r^2) + \tfrac{1}{2}r_\tau^2(r^2 - r\, r_\tau)(1 - s^2) \qquad \tau = 2, 4, 6, 8 \\ F_\tau = (1 - r^2)(1 - s^2) \qquad \tau = 9 \end{gathered} \tag{7}$$

Using LE the unknowns are only the displacements of the cross-sectional nodes.

2.1.2 Finite Elements (FE) solution

The FEM is used to approximate the displacement along the beam axis. In particular, the generalized displacement vector, $u_\tau(y)$, is linearly interpolated using the classical shape functions. When a beam element with N_{NE} nodes along the axis is considered, the generalized displacement vector becomes:

$$\mathbf{u}_\tau(y) = N_i(y)\mathbf{q}_{i\tau}; \qquad i = 1 \dots N_{NE} \tag{8}$$

In Eq. 8 the index i ranges from 1 to the number of nodes per element N_{NE}. Therefore, the displacement field can be written as follows:

$$\mathbf{u}(x, y, z) = F_\tau(x, z)N_i(y)\mathbf{q}_{i\tau} \tag{9}$$

Where index i indicates the node of the element along the y-axis. Three- and four-node refined beam elements were used along the y-axis in the present work.

2.2 Governing equations

The governing equations are derived using the Principle of Virtual Displacements (PVD) that in the dynamic case assumes the following form:

$$\delta L_{int} = \delta L_{ext} - \delta L_{ine} \tag{10}$$

Where L_{int} stands for the strain energy, L_{ext} is the work of the external loadings, and L_{ine} is the work of the inertial loadings. δ denotes the virtual variation. In the case of free vibration analysis, the work of the external loadings is equal to zero, Eq. 10 becomes:

$$\delta L_{int} + \delta L_{ine} = 0 \tag{11}$$

The internal work can be written as:

$$\delta L_{int} = \int_V \delta\boldsymbol{\epsilon}^T \boldsymbol{\sigma} dV \tag{12}$$

By introducing the constitutive equations and the geometrical relations given respectively in Eq.3 and Eq.2 and introducing the displacement field given in Eq. 9, the variation of the internal work becomes:

$$\delta L_{int} = \delta\mathbf{q}_{\tau i}^T \int_V \left[N_i(y)F_\tau(x, z) \;\; \boldsymbol{D}^T \;\; \boldsymbol{C} \;\; \boldsymbol{D} \;\; F_s(x, z)N_j(y) \right] dV \mathbf{q}_{sj} \tag{13}$$

The differential matrix $\boldsymbol{D}$ operates on F_τ, F_s, N_i and N_j. By splitting the integral on the volume V in two sub-integral, one on the cross-section Ω and one along the beam axis l one has:

$$\begin{aligned}
\delta L_{int} =& \delta\mathbf{q}_{\tau i}^T \left\{ \int_{\boldsymbol{V}} \left[\left(\boldsymbol{D}_\Omega + \boldsymbol{D}_y \right)^T F_\tau(x, z) \;\; N_i(y) \;\; \mathbf{I} \right] \;\; \boldsymbol{C} \;\; \left[\left(\boldsymbol{D}_\Omega + \boldsymbol{D}_y \right) N_j(y) \;\; F_s(x, z) \;\; \mathbf{I} \right] \right\} dV \mathbf{q}_{sj} \\
=& \delta\mathbf{q}_{\tau i}^T \left\{ \int_l \left(N_i(y) \left[\int_\Omega \left[\boldsymbol{D}_\Omega \;\; F_\tau(x, z) \;\; \mathbf{I} \right] \;\; \boldsymbol{C} \;\; \left[\boldsymbol{D}_\Omega \;\; F_s(x, z) \;\; \mathbf{I} \right] d\Omega \right] N_j(y) \;\; \right) dy \right. \\
&+ \int_l \left(N_i(y) \left(\int_\Omega \left[D_\Omega^T \;\; (F_\tau(x, z) \;\; \mathbf{I}) \right] \;\; \boldsymbol{C} \;\; F_s(x, z) \;\; d\Omega \right) D_y \;\; (N_j(y) \;\; \mathbf{I}) \right) \;\; dy \\
&+ \int_l \left(D_y^T \;\; (N_i(y) \;\; \mathbf{I}) \left(\int_\Omega F_\tau(x, z) \;\; \boldsymbol{C} \;\; \left[D_\Omega \left(F_s(x, z) \;\; \mathbf{I} \right) \right] d\Omega \right) \;\; N_j(y) \;\; \right) dy \\
&\left. + \int_l \left(D_y^T \;\; (N_i(y) \;\; \mathbf{I}) \left(\int_\Omega F_\tau(x, z) \;\; \boldsymbol{C} \;\; F_s(x, z) d\omega \right) D_y \;\; (N_j(y) \;\; \mathbf{I}) \, dy \right\} \mathbf{q}_{sj} \right. \\
=& \;\; \delta\mathbf{q}_{sj}^T \;\; \boldsymbol{K}^{ij\tau s} \;\; \mathbf{q}_{\tau i}
\end{aligned} \tag{14}$$

Where $\boldsymbol{K}^{ij\tau s}$ is the stiffness matrix expressed in form of "*fundamental nucleus*" that is a 3×3 array. $\mathbf{q}_{\tau i}$ is the vector of the nodal unknown and $\delta\mathbf{q}_{sj}$ is its virtual variation. $\mathbf{I}$ is the identity matrix. The explicit form of the fundamental nucleus can be found in [30].

The virtual variation of the work of the inertial loadings is:

$$\delta L_{ine} = \int_V \delta\mathbf{u}^T \ \rho \ \ddot{\mathbf{u}} \ \ dV \tag{15}$$

where $\ddot{\mathbf{u}}$ stands the acceleration vector and ρ is the density of the material. The Eq.15 can be rewritten using Eq.4:

$$\delta L_{ine} = \delta\mathbf{q}_{sj}^T \int_l N_i(y) \left\{ \int_\Omega \rho \left[F_\tau(x,z) \ \ \mathbf{I}\right] \left[F_s(x,z) \ \ \mathbf{I}\right] d\Omega \right\} N_j(y) dz \ddot{\mathbf{q}}_{\tau i} = \delta\mathbf{q}_{sj}^T \ \ \boldsymbol{M}^{ij\tau s} \ \ \ddot{\mathbf{q}}_{\tau i} \tag{16}$$

Where the mass matrix $\boldsymbol{M}^{ij\tau s}$ is a 3×3 *fundamental nucleus*, where the indices have the same meaning of those of stiffness matrix.

In conclusion, the PVD can be written as following:

$$\delta\mathbf{q}_{sj}^T \left(\boldsymbol{K}^{ij\tau s} \ \ \mathbf{q}_{\tau i} + \boldsymbol{M}^{ij\tau s} \ \ \ddot{\mathbf{q}_{\tau i}}\right) = 0 \tag{17}$$

The global stiffness and mass matrices are obtained by means of the classical FE assembling procedure, as shown in [30]. The equation for a free undamped problem can be written as:

$$\boldsymbol{M}\ddot{\boldsymbol{q}} + \boldsymbol{K}\boldsymbol{q} = 0 \tag{18}$$

Where $\boldsymbol{q}$ is the global unknowns vector. Due to linearity of the problem, harmonic solutions are possible and the natural frequencies, ω_k, are obtained by solving the following eigenvalues problem:

$$\left(-{\omega_k}^2 \boldsymbol{M} + \boldsymbol{K}\right) \boldsymbol{q}_k = 0 \tag{19}$$

Where $\boldsymbol{q}_k$ is the *k-th* eigenvector, and k ranges form 1 to total numbers of DOF of the structures. Non-structural masses can be arbitrarily located in the 3D domain of the beam structure. In the framework of the Carrera Unified Formulation, this is realized by adding the following term to the fundamental nucleus of the mass matrix:

$$\mathbf{m}^{ij\tau s} = \mathbf{I} \left[F_\tau(x_m, z_m) F_s(x_m, z_m) N_i(y_m) N_j(y_m)\right] \widetilde{m} \tag{20}$$

where $\mathbf{I}$ is the 3×3 identity matrix, while $\widetilde{m}$ represents the non-structural mass placed at the point (x_m,y_m,z_m).

3 Numerical Results

In this section, different space structures made of composite materials have been considered. For the assessment, the static and the dynamic response of an eight layers composite beam structure has been investigated. The first thin-walled reinforced structure analysed is a composite cylinder reinforced using eight stringers along the longitudinal direction and a rib located at half length. The second case concerns an outline of a launcher with a shape similar to the Arian V, the launcher from the European Space Agency. In this last case, the configuration at the take-off, with the solid and cryogenic masses and the payload mass, is used to investigate the effect of the masses on the on the free vibration analysis.

4 Preliminary Assessment

The finite element analysis of a composite beam component is reported as assessment. The geometrical properties are shown in Fig.2a, where also the information about the material lamination are included. The cantilever beam is loaded at the tip by a concentrated load with a magnitude of 0.2 N. The beam is composed of 8 layers, and each layer has the same thickness and equal to 0.00125 [mm]. The orthotropic material considered has a longitudinal Young's modulus equal to 30 GPa while the transversal modlulus is equal to 5GPa. The shear modulus are considered equal to 1 GPa while the Poisson's ratios equal to 0.25. Two lamination have been used, the layers in which has been used the material 1 have a lamination angle of 0^o while a 90^0 angle has been used in material 2. The LE model is realized using $8 - B4$ elements on the

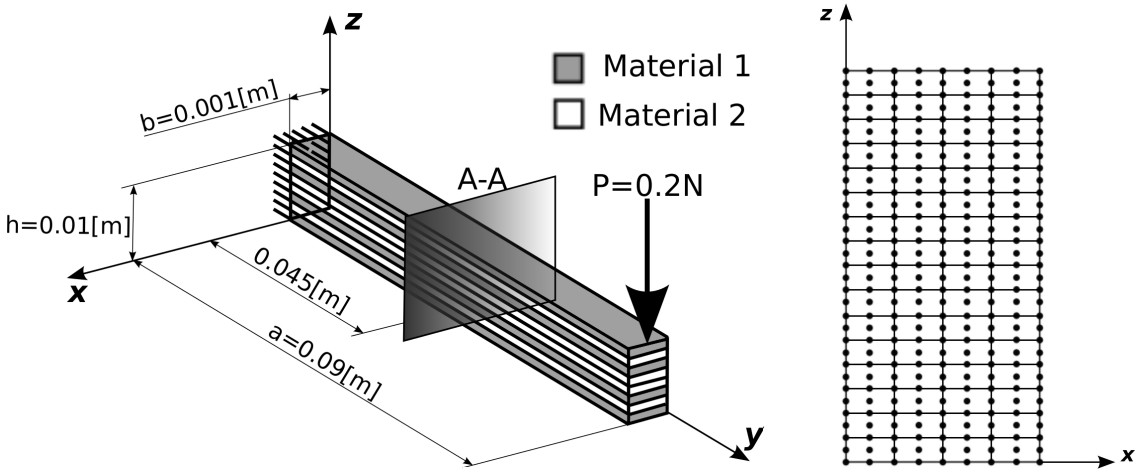

(a) *Global properties* (b) *LE 1D Cross-Section*

Figure 2: Cantilever composite beam.

$y - axis$ and the cross-section is modelled using 64 LE elements as shown in Fig.2b. The results compared are related to the vertical displacement $u_z = u_z(a, b/2, h/2)$, the principal stress $\sigma_{yy} = \sigma(yy)(a/2, b/2, h)$ and the transversal shear stress $\sigma_{yz} = \sigma(yz)(a/2, b/2, h/2)$. Tab.1 shows the results al the points above mentioned related to different models. The results have been compared with those from the analytical solution proposed by Lekhnitskii [31], this reference solution has also been used to compare the stresses σ_{yy} and σ_{yz} shown in the Figures 3a and 3b, respectively. The results related to the LE model is included in the same table and it is labelled LE. The results shown in Fig.3 highlighting the capabilities of the present one-dimensional model to

deal with laminated structured. An accurate description of the displacement, normal stress and shear stress fields can be achieved.

Model	$-u_z \times 10^2[mm]$	$\sigma_{yy} \times 10^3[MPa]$	$\sigma_{yz} \times 10^2[MPa]$
Lekhnitskii (1968) [31]	-	730	2.789
Surana and Nguyen (1990) [32]	3.031	720	-
Davalos and KimBarbero (1994) [33]	3.029	700	-
Xiaoshan Lin (2011) [34]	3.060	750	-
Vo and Thai (2012) [35]	3.024	-	-
LE CUF	3.029	734	2.791

Table 1: Deflection and stresses of the laminated beam model.

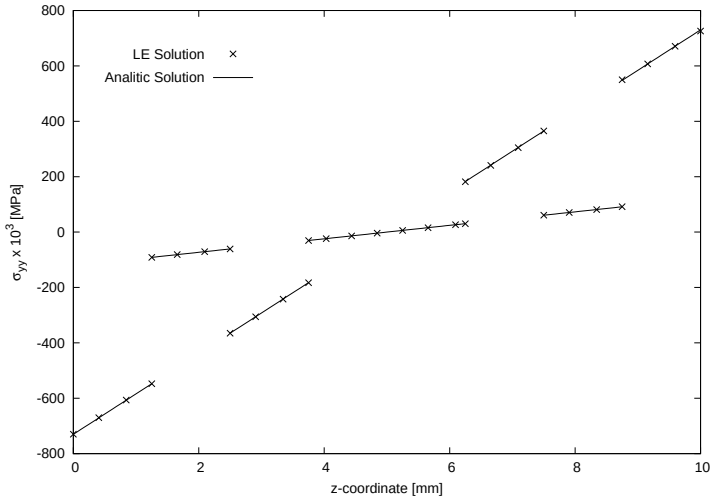

(a) σ_{yy}

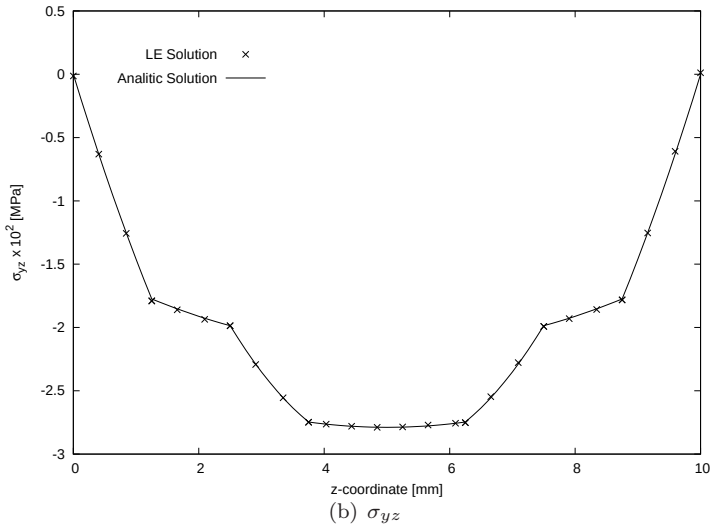

(b) σ_{yz}

Figure 3: Stress along the z-coordinate in $x = b/2$ and $y = a/2$.

A solid FE model from the commercial Nastran code is used to compare the results of the present refined one-dimensional model in the free vibration analysis. The Modal Assurance Criterion (MAC) is used to compare the results. The MAC, is defined as a scalar number that represents the degree of consistency between two vectors (see [36]):

$$MAC_{ij} = \frac{\left|\{\phi_{A_i}\}^T\{\phi_{B_j}\}\right|^2}{\{\phi_{A_i}\}^T\{\phi_{A_i}\}\{\phi_{B_j}\}\{\phi_{B_j}\}^T} \tag{21}$$

where, $\{\phi_{A_i}\}$ is the i^{th}-eigenvector of model A, while $\{\phi_{B_j}\}$ is the j^{th}-eigenvector of model B. MAC can ranges from zero (when two modes are completely different) to 1 (when the maximum correspondence between two modes is achieved). Different tonalities of gray appear when two modes correspond not perfectly.

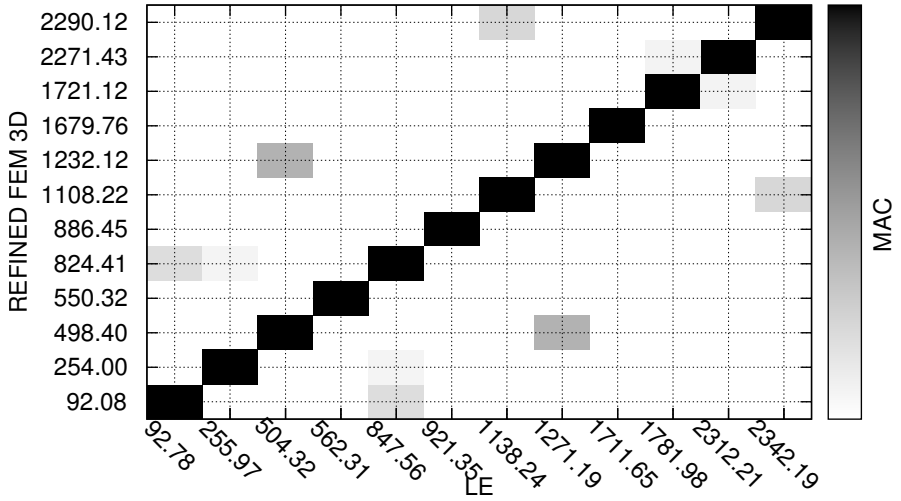

Figure 4: MAC between $3D - FE$ model and $LE - CUF$ model.

$Mode$	FEM_{3D}	$LE - CUF$
DOF	155379	22275
1	92.08	92.78 $^{(+0.7\%)}$
2	254.00	255.97 $^{(+0.8\%)}$
3	498.40	504.32 $^{(+1.2\%)}$
4	550.32	562.31 $^{(+2.2\%)}$
5	824.41	847.56 $^{(+2.8\%)}$
6	886.45	921.35 $^{(+3.9\%)}$
7	1108.22	1138.24$^{(+2.7\%)}$
8	1232.12	1271.19$^{(+3.2\%)}$
9	1679.76	1711.65$^{(+1.9\%)}$
10	1721.12	1781.98$^{(+3.5\%)}$
11	2271.41	2312.21$^{(+1.8\%)}$
12	2290.12	2342.19$^{(+2.3\%)}$

$(\,)^{(*\%)}$: $*$ *percentage different to* FEM_{3D}

Table 2: First 12 no-rigid frequencies.

Tab.2 shows the values of the first 12 natural frequencies evaluated using different approaches. The LE model is able to provide an error lower of 4 % on the modes considered but the LE DOFs uses only the 14% of the $3D - model$ DOFs. Fig.5 shows the first and second bending and torsional modes evaluated using the $1D - CUF$ model.

5 Composite reinforced Cylinder

The geometry of the structure considered is shown in Fig.6, and the informations about the cross-sections are shown in Fig.7. Along the beam axis, three components are joined together using the component-wise

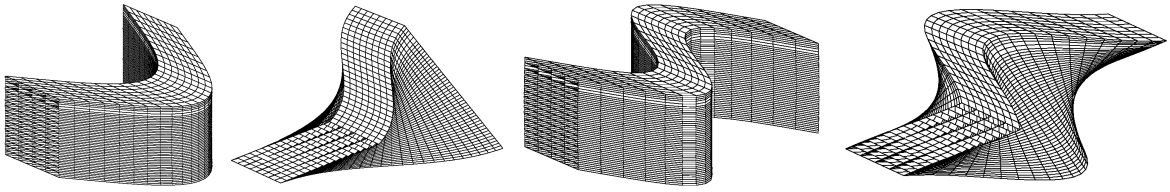

(a) $f1 = 92.78$ (b) $f2 = 255.97$ (c) $f3 = 504.32$ (d) $f4 = 562.31$

Figure 5: First and second bending and torsional modes.

approach. A metallic material is used for the rib and the stringers, while an orthotropic material is used for the skins. In particular, the component made using a metallic material are characterised by a Young modulus value, E, equal to 75 GPa, the Poisson ratio, ν, is equal to 0.3 and the density value, ρ, is equal to 2700 kg/m^3. The orthotropic material has the following properties: E_{LL} = 142 GPa, $E_T = E_Z$ = 9.8 GPa, G_{TZ} = G_{LZ}=6 GPa, G_{LT}= 4.83 GPa, $\nu_{TZ} = \nu_{LZ}$= 0.42, ν_{LT}= 0.5 and ρ = 1445 kg/m^3.

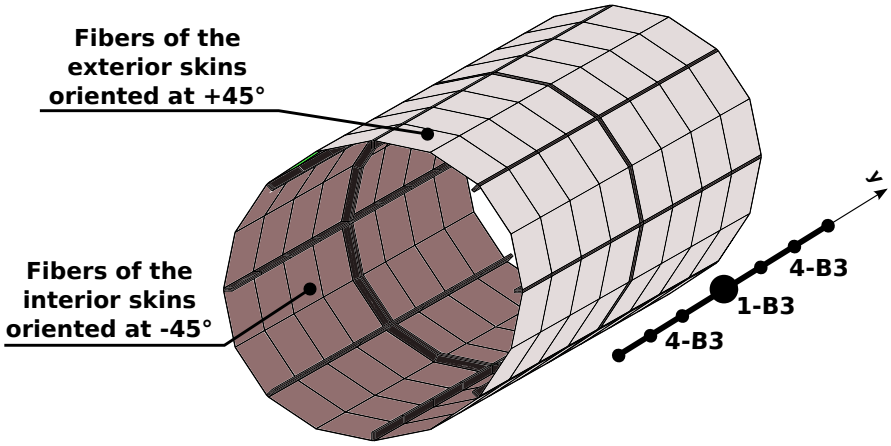

Figure 6: Layout of the reinforced cylindrical structure.

$4 - B3$ beam elements are used for the first and for the last thin-walled components, while only $1 - B3$ beam element is used for the second component, a transversal stringer.

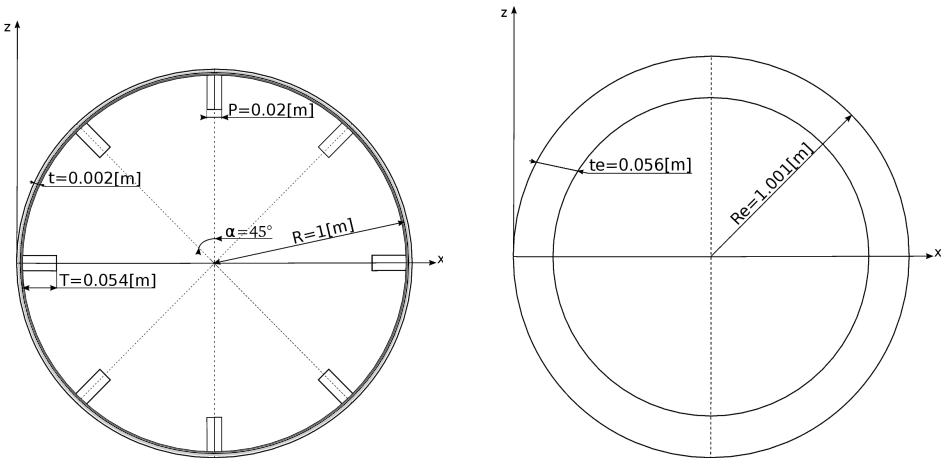

(a) *Thin-walled reinforced components* (b) *Rib component*

Figure 7: Cross-section geometrical properties.

The skin thickness is divided into two layers with equal thickness, as shown in Fig.8b. Two different fiber

orientations are considered for the skins, in particular the fibers for the outer skins are oriented with an angle of +45°, while the fibers of the inner skins have an angle of -45°, as shown in Fig.6.

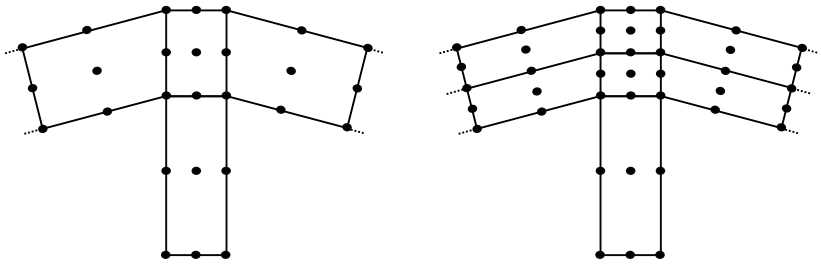

(a) *Thin-walled metallic reinforced cylinder*

(b) *Thin-walled composite reinforced cylinder*

Figure 8: Lagrange elements configuration for the isotropic and composite case.

Tab.4 shows the results about four different FE models. First of all a fully isotropic structure has been considered. In this case the isotopic material used for the stringers has been used also for the skin. The first three column reports the results for this structure. In particular, the first two columns report the results from two FE models obtained using the commercial Nastran code. A solid refined model called $FEM-3D$ has a very high number of DOFs and its results are used as reference solution. The second FE model is a shell-beam model, called $FEM\ 2D-1D$, where shell elements are used for the skins and beam elements for the stringers with the off-set. The third column contains the $1D-CUF$ model, called LE from Lagrange Expansion. The skins of the $LE_{ISOTROPIC}$ model does not have two layer, as shown in Fig.8a, in fact the $LE_{ISOTROPIC}$ DOFs are lower than the $LE_{COMPOSITE}$ DOFs. 32 LE elements are used for the cross-section of the $LE_{ISOTROPIC}$ model, while 56 LE elements are used for the $LE_{COMPOSITE}$ model. Further information about the FE models above mentioned are shown in the work [28].

Mode	FEM_{3D}	FEM_{2D-1D}	$LE_{ISOTROPIC}$	$LE_{COMPOSITE}$
DOF :	390192	26206	8352	16848
Bending	Frequencies [Hz]:			
1^a	33.64	37.49 $^{(+11.4\%)}$	34.23 $^{(+1.7\%)}$	34.16
2^a	94.82	91.06 $^{(-4.0\%)}$	93.85 $^{(-1.0\%)}$	101.31
Torsional	Frequencies [Hz]:			
1^a	67.67	77.83 $^{(+15.0\%)}$	73.18 $^{(+8.1\%)}$	90.90
2^a	175.33	179.49$^{(+2.4\%)}$	174.61$^{(-0.4\%)}$	283.49

$(\ )^{(*\%)}$: $*$ *percentage different with respect to* FEM_{3D}

Table 3: First two bending and torsional frequencies for different FE models.

Tab.4 shows that using the advanced composite layout, the main effects can be seen on the torsional frequencies, as expected. In fact in this case the bending frequencies are about the same with respect to those obtained using the metallic structure. In contrast the torsional frequencies are increased, in particular the first torsional frequency is now 25% higher than that obtained in the isotropic case, while the second torsional torsional frequency is now 62% higher than in the case with only metallic material.

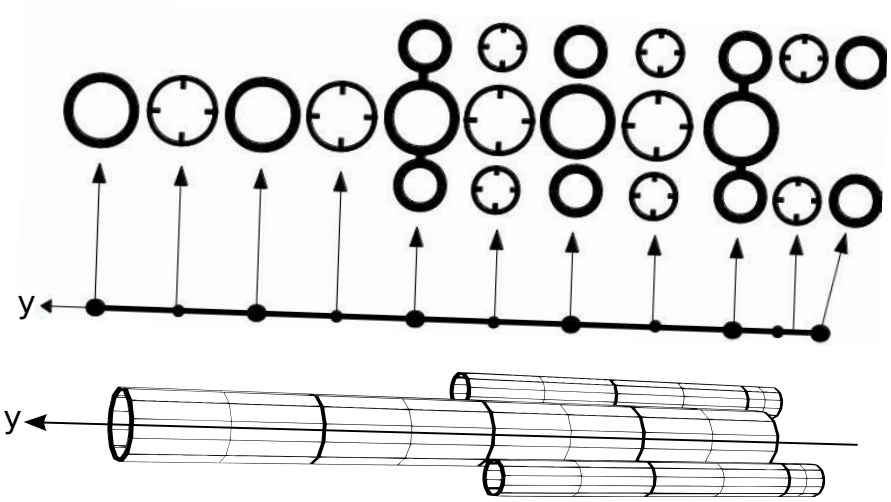

Figure 9: From Solid Model to One-dimensional Model.

6 Composite Empty launcher

Figure 9 shows the geometry of the launcher model analyzed. It's shape is similar to the Arian V, European launcher, with a central body and two later boosters. The total length is 59 meters. According to FEM approximation along the $y-axis$, the 11 components joined together are modelled using different beam elements, in particular, $2-B3$ beam elements are used for the thin-walled reinforced components, while only $1-B3$ beam element is used to model the rib components. The cross-section geometrical properties can be found in [28] where the $1D-CUF$ (or LE) metallic model is compared with respect to two FE models from the commercial Nastran code, a $shell-beam$ FE model and a $Solid\ Refined$ model. An advanced assessment analysis was conduced recently in [29] where the metallic LE launcher model is compared with respect to a $Solid$ FE model using the same DOFs, as shown in the first three columns of the Tab.4. Tab.4 is built using the MAC. A metallic material is used for the rib and the stringers, while an orthotropic material is used for the skins. In particular, the components made using a metallic material are characterised by a Young modulus value, E, equal to 75 GPa, the Poisson ratio, ν, is equal to 0.3 and the density value, ρ, is equal to 2700 kg/m^3. The orthotropic material has the following properties: E_{LL} = 142 GPa, $E_T = E_Z$ = 9.8 GPa, $G_{TZ} = G_{LZ}$=6 GPa, G_{LT}= 4.83 GPa, $\nu_{TZ} = \nu_{LZ}$= 0.42, ν_{LT}= 0.5 and ρ = 1445 kg/m^3.

The composite launcher has the same composite layout used for the thin-walled reinforced cylinder, the isotropic material is used for the stringers and for the ribs, while the mentioned orthotropic material is adopted for the skins. The skins have two layers with the same thickness to include two different fiber orientations following the schema shown in Fig.10

Also in this case an assessment has been performed on the fully isotropic model. The results show the accuracy provided by the present model. If compared with a three-dimensional model with the dame DOFs the present model appears to provide more accurate results. Using the composite layout the frequencies increase with respect to the case with only metallic material, as shown in the last column of the Tab.4.

Fig.11 shows some modal shape obtained using the LE refined model. Fig.11a shows the local modes of both the booster, while in Fig.11b is shown the local mode of the right booster. The global bending mode is shown in Fig.11c. The $1D-CUF$ models are also capable to include very complex shell-like modes, as shown

MODE DOF	$REF\ FEM-3D$ 197436	$FEM-3D$ 29628	$LE_{ISOTROPIC}$ 29628	$LE_{COMPOSITE}$ 42876
1	0.73	0.75 $^{(+2.7\%)}$	0.74 $^{(+1.4\%)}$	0.76
2	0.90	0.93 $^{(+3.3\%)}$	0.92 $^{(+2.2\%)}$	0.95
3	4.55	5.20 $^{(+14.3\%)}$	4.70 $^{(+3.3\%)}$	4.82
4	6.60	7.65 $^{(+15.9\%)}$	6.84 $^{(+3.6\%)}$	6.37
5	7.76	8.02 $^{(+3.4\%)}$	7.94 $^{(+2.3\%)}$	6.40
6	7.92	7.96 $^{(+0.5\%)}$	8.05 $^{(+1.6\%)}$	6.95
7	8.38	9.23 $^{(+10.1\%)}$	8.53 $^{(+1.8\%)}$	9.03
8	8.66	9.65 $^{(+11.4\%)}$	8.95 $^{(+3.3\%)}$	9.13
9	9.00	10.08$^{(+12.0\%)}$	9.23 $^{(+2.6\%)}$	9.84
10	9.45	10.83$^{(+14.6\%)}$	9.70 $^{(+2.6\%)}$	10.06
11	10.21	11.54 $^{(+13.0\%)}$	10.71 $^{(+4.9\%)}$	10.61
12	10.35	11.59 $^{(+12.0\%)}$	10.55 $^{(+1.9\%)}$	10.87
13	12.06	12.54 $^{(+4.0\%)}$	12.49 $^{(+3.6\%)}$	11.75
14	12.09	12.37 $^{(+2.3\%)}$	12.50 $^{(+3.4\%)}$	12.61
15	13.49	15.31 $^{(+13.5\%)}$	14.01 $^{(+3.9\%)}$	14.06

$(\ )^{(*\%)} : * \ percentage\ different\ with\ respect\ to\ REF\ FEM-3D$

Table 4: First 15 no-rigid frequencies for different FE models.

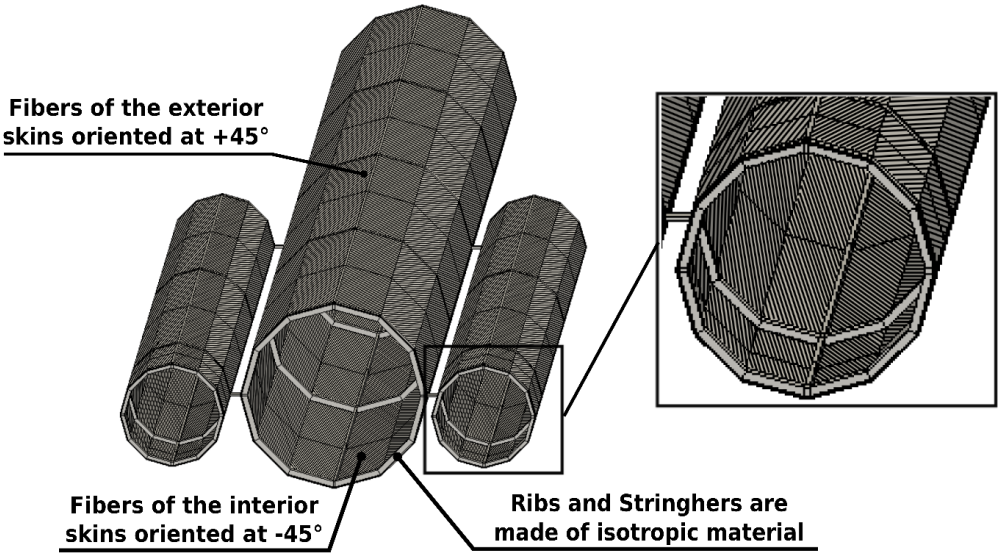

Figure 10: Composite layout for the launcher structure.

in Fig.11d.

(a) *Mode 1* (b) *Mode 5* (c) *Mode 13* (d) *Mode 15*

Figure 11: Different modal shapes of the composite launcher.

7 Full Composite launcher configuration

In this section, the composite launcher analyzed previously, is studied including additional masses present during the take-off phase. As shown in [37], at the take-off the whole mass added can be schematize as shown in Fig.12. The solid fuel is contained in the lateral boosters, while the central body contains the cryogenic fuel. In the top of the launcher there is the pay-load. Solid, cryogenic and pay-load masses can be added as non-structural masses in the model. Each mass is located at the central node on the free-edge of the stringers , see Figure Fig.12b, and they are spaced equally at about 3.375 [m] along the y direction.

7.1 Comparison between Empty and Full Composite launcher

Tab.5 shows the first fifteen no-rigid frequencies when the fuel and the pay-load masses are added to the empty launcher. The first effect concerns the frequencies reduction. In fact if the whole stiffness does not change and the mass increases, the frequencies decrease, as highlighted in the column related to the full launcher in Tab.5.

Fig.13 contains the comparison between the empty and full composite launcher. The results show that the first three modes do not change the modal shape, MAC$\approx$1, but the frequencies are strongly reduced. The effects of the masses have a strong impact on all the other modes, that is, many of them are shifted with respect the empty configuration. Many local models appears earlier than the global banding mode, in fact it is mode 8 in the full configuration while it was mode 5 in the empty launcher case. These results show that the effect of the masses may have a strong impact not only on the frequency values but also on the modal shape.

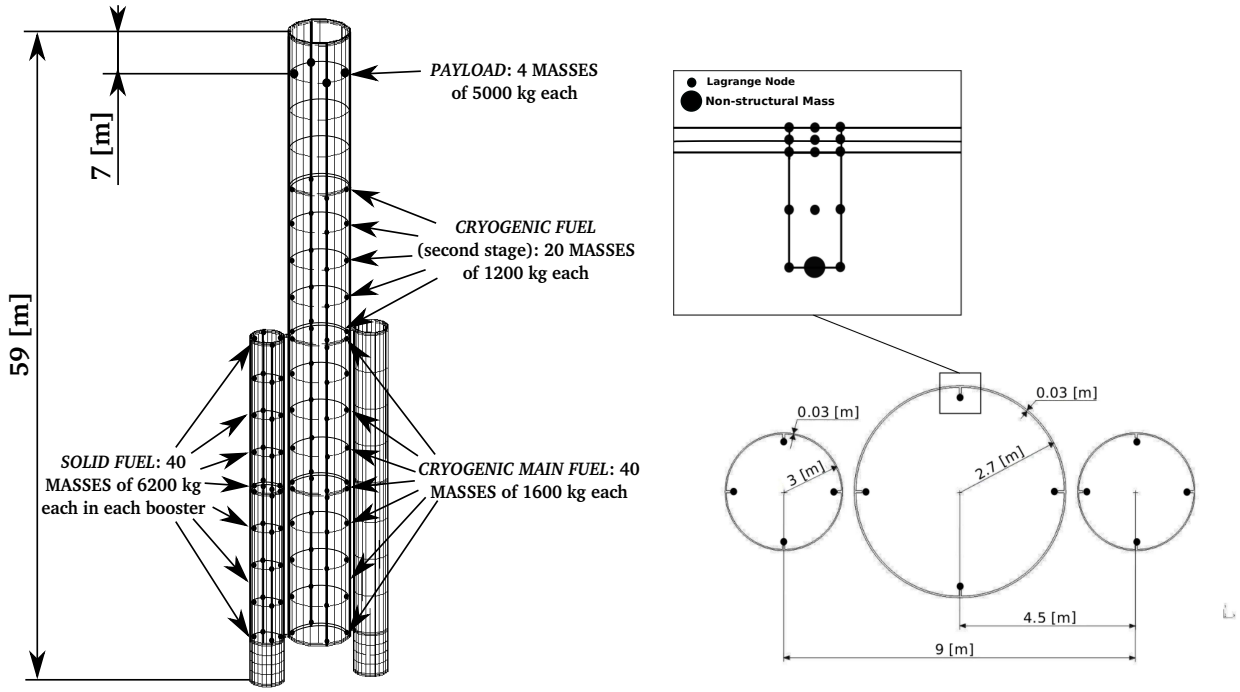

(a) *Global Configuration* (b) *Local Masses location*

Figure 12: Fuel and Payload Mass at take-off.

MODE DOF	*Empty* 42876	*Full* 42876
1	0.76	0.28
2	0.95	0.42
3	4.82	1.63
4	6.37	2.71
5	6.95	3.34
6	9.03	3.87
7	9.13	4.06
8	9.84	4.10
9	10.06	4.29
10	10.61	4.37
11	10.87	4.39
12	11.75	4.59
13	12.61	4.72
14	14.06	5.08
15	14.33	5.70

Table 5: First 15 no-rigid frequencies for different composite launcher configurations.

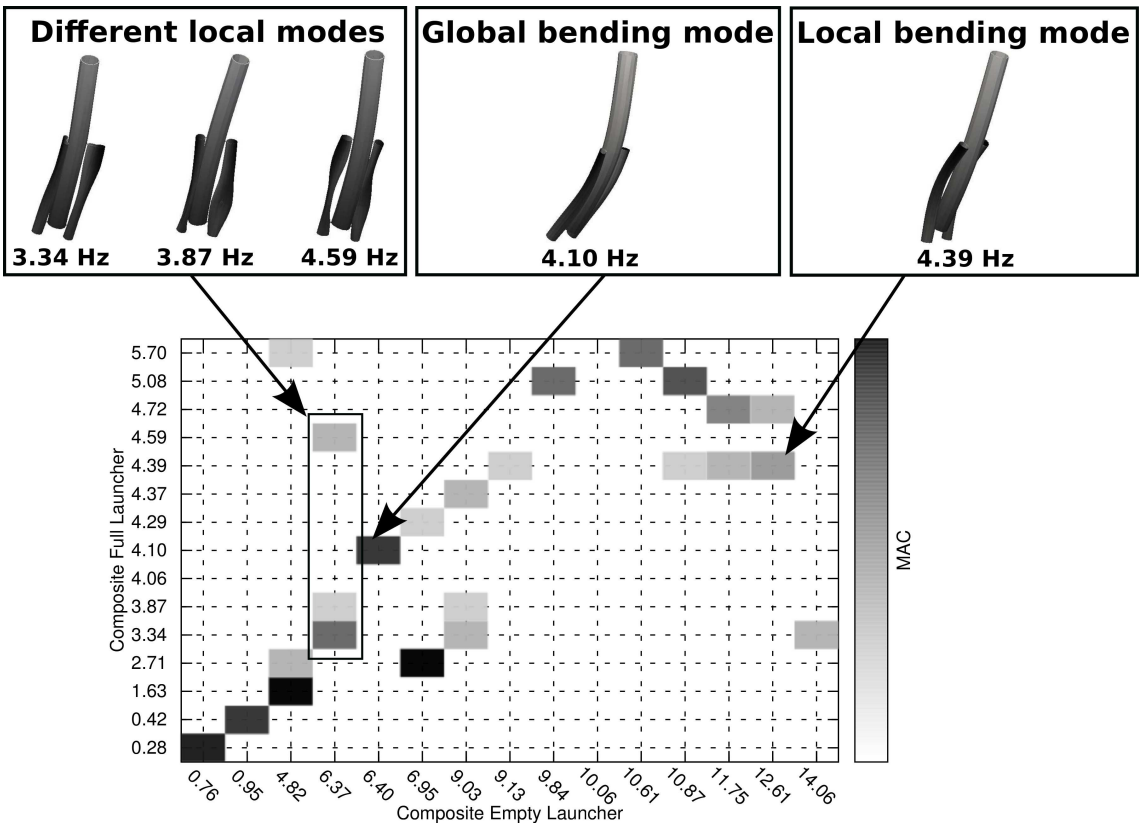

Figure 13: MAC analysis: full VS empty composite launcher.

8 Concluding Remarks

In the present work, the effect of composite materials and non-structural masses on the free vibration analysis of simple and complex space vehicle have been analysed. A one-dimensional refined model was derived using the Carrera Unified Formulation, based on the Lagrange expansion. Two reinforced structures have been taken into account in the analysis: a thin-walled cylinder reinforced using eight longitudinal stringers and one transversal rib and an outline of a launcher with a central body and two lateral boosters. Different FE models from the commercial Nastran® code have been used to compare different results.

From the analysis performed, the following conclusions can be drown:

- the refined one-dimensional models permits to analyse reinforced structures overcoming the limits of the classical one-dimensional models;
- the present 1D model makes it possible to analyse both plate and stringers using the same element, in addition, global and local modes (shell-like) can be described;
- the LE models providea quasi three-dimensional solution with a lower computational cost than the solid models;
- composite materials and non-structural masses can be included in the present refined one-dimensional model;
- composite material increase frequencies when an appropriate layout of the fibers is used, but also the DOFs numberr increases;

In conclusion, the refined CUF models are very attractive in the analysis of complex reinforced space structures. Extension to more complex cases, as well as the effect on the frequencies due to a load factor, could be an important extension of the proposed investigation. In addition, an advanced model with node-kinematics variable can be also used to reduce the total DOFs.

References

[1] S.P. Timoshenko. *Theory of Plates and Shells, 2nd ed.* McGraw-Hill, 1959. New York.

[2] A. Deb and Booton M. Finite element models for stiffened plates under transverse loading. *Computers and Structures*, 8(3):361–372, 1988.

[3] C.W. Bert, S.K. Jang, and A.G. Striz. Nonlinear bending analysis of orthotropic rectangular plates by the method of differential quadrature. *Computational Mechanics*, 5(2/3):217–226, 1989.

[4] J. Farsa, A.R. Kukreti, and C.W. Bert. Fundamental frequency analysis of single spacially orthotropic, generally orthotropic and anisotropic rectangular layered plates by differential quadrature method. *Computers and Structures*, 46(3):465–477, 1993.

[5] F. Civan. Solving multivariable mathematical models by the quadrature and cubature methods. *Numerical Methods for Partial Differential Equations*, 10:545–567, 1994.

[6] A. Leissa. *Vibration of Plates.* Acoustical Society of America, 1993. New York.

[7] A. Leissa. *Vibration of Shells.* Acoustical Society of America, 1993. New York.

[8] M. C. Junger and D. Feit. *Sound, Structures and Their Interaction. 2nd ed.* Acoustical Society of America, 1993. New York.

[9] M.J. Turner, R.W. Clough, H.C. Martin, and L.J. Topp. Stiffness and Deflection Analysis of Complex Structures. *Journal of the Aeronautical Sciences*, 23(9):805–823, sep 1956.

[10] A. Hrennikoff. Solution of problems of elasticity by the framework method. *Journal of applied mechanics*, 12:169–175, 1941.

[11] R. Courant. Variational methods for the solution of problems of equilibrium and vibrations. *Bulletin of the American Mathematical Society*, 43:1–23, 1943.

[12] G. Strang and G. Fix. *An Analysis of the Finite Element Method.* 1973.

[13] R. D. Buehrle, G. A. Fleming, and R. S. Pappa. Finite element model development and validation for aircraft fuselage structures. *18-th international Modal Analysis Conference.*, 2000. San Antonio, Texas.

[14] G. Durin, F. Bouvier, G. Mastrangelo, and E. Robert. Ariane 5 solid rocket booster dynamic behaviour with respect to pressure oscillation. *Propulsion Physics*, 2:149–162, 2011.

[15] N. Merlette and E. Pagnacco. Structural dynamics of solid propellants with frequency dependent properties. *12-th European Conference os Space Structures, Materials & Enviromental Testing.*, 2012. Noordwijk, The Netherlands.

[16] E. Carrera and G. Giunta. Refined beam theories based on a unified formulation. *Int. J. Appl. Mech.*, 2(1):117–143, 2010.

[17] E. Carrera, G. Giunta, P. Nali, and M. Petrolo. Refined beam ele-ments with arbitrary cross-section geometries. *Comput. Struct.*, 88(5–6):283–293, 2010.

[18] E. Carrera, M. Petrolo, and P. Nali. Unified formulation applied to free vibrations finite element analysis of beams with arbitrary section. *Shock Vib.*, 18(3):485–502, 2011.

[19] E. Carrera, M. Cinefra, M. Petrolo, and E. Zappino. Comparisons between 1d (beam) and 2d (plate/shell) finite elements to analyze thin walled structures. *Aerotecnica Misssili & Spazio. The journal of Aerospace Science, Technology and Systems*, 93(1-2), 2014.

[20] E. Carrera and G. Giunta. Refined beam theories based on a unified formulation. *International Journal of Applied Mechanics*, 2(1):117–143, 2010.

[21] E. Carrera, G. Gaetano, and Petrolo M. *Beam Structures, Classical and Advanced Theories.* John Wiley & Sons, 2011.

[22] E. Carrera, A. Pagani, and M. Petrolo. Classical, refined and component-wise analysis of reinforced-shell structures. *AIAA Journal*, 51(5):1255–1268, 2013.

[23] E. Carrera, A. Pagani, and M. Petrolo. Component-wise method applied to vibration of wing structures. *Journal of Applied Mechanics*, 88(4):041012–1–041012–15, 2013.

[24] G. Giunta, F. Biscani, S. Belouettar, A. J. M. Ferreira, and E. Carrera. Free vibration analysis of composite beams via refined theories. *Composite Part B*, 44(1):540–552, 2013.

[25] T. Cavallo, E. Zappino, and E. Carrera. Component-wise vibration analysis of stiffened plates accounting for stiffener modes. *CEAS Aeronautical Journal*. in press.

[26] E. Carrera, E. Zappino, and T. Cavallo. Static analysis of reinforced thin-walled plates and shells by means of various finite element models. *nternational Journal for Computational Methods in Engineering Science and Mechanics*, 17(2):106–126, 2016.

[27] E. Zappino, T. Cavallo, and E. Carrera. Free vibration analysis of reinforced thin-walled plates and shells through various finite element models. *Mechanics of Advanced Materials and Structures*, 23(9):1005–1018, 2015.

[28] E. Carrera, E. Zappino, and T. Cavallo. Accurate free vibration analysis of launcher structures using refined 1d models. *International Journal of Aeronautical and Space Sciences*, 16(2):206–222, 2015.

[29] E. Carrera, E. Zappino, and T. Cavallo. Effect of solid mass consumption on the free-vibration analysis of launchers. *Journal of Spacecraft and Rockets (AIAA)*. In press.

[30] E. Carrera, M. Cinefra, M. Petrolo, and E. Zappino. *Finite Element Analysis of Structures Through Unified Formulation.* John Wiley & Sons, 2014.

[31] S. G. Lekhnitskii. *Anisotropic Plates.* TGordon and Branch, 1968.

[32] S. H. Nguyen and K. S. Surana. Two-dimensional curved beam element with higher-order hierarchical transverse approximation for laminated composites. *Composite and Structures*, 36:499–511, 1990.

[33] J. F. Davalos, Y. Kim, and Barbero E. J. Analysis of laminated beams with a layerwise constant shear theory. *Composite and Structures*, 28:241–253, 1994.

[34] Y. Z. Xiaoshan Lin. A novel one-dimensional two-node shear-flexible layered composite beam element. *Finite Elements in Analysis and Design*, 47:676–682, 2011.

[35] T. P. Vo and H. T. Thai. Static behavior of composite beams using various refined shear deformation theories. *Composite and Structures*, 94:2513–2522, 2012.

[36] R. J. Allemang and D. L. Brown. A correlation coefficient for modal vector analysis. *Proceedings of the 1st SEM International Modal Analysis Conference*, pages 110–116, 1982. Orlando, FL, November 8-10.

[37] Edouard Perez Senior Vice President Engineering. *Ariane 5, Users Manual.*, volume 5. arianespace service & solutions, 2011.